Energy cascade and its locality in compressible magnetohydrodynamic turbulence

Yan Yang, Yipeng Shi, Minping Wan, William H. Matthaeus, and Shiyi Chen

Phys. Rev. E **93**, 061102 — Published 24 June 2016

DOI: 10.1103/PhysRevE.93.061102

Energy cascade and its locality in compressible magnetohydrodynamic turbulence

Yan Yang,[1,2] Yipeng Shi,[1,*] Minping Wan,[3,†] William H. Matthaeus,[2] and Shiyi Chen[1,3,4]

[1]*State Key Laboratory for Turbulence and Complex Systems, Center for Applied Physics and Technology, College of Engineering, Peking University, Beijing 100871, P. R. China*

[2]*Department of Physics and Astronomy, University of Delaware, Newark, DE 19716, USA*

[3]*Department of Mechanics and Aerospace Engineering, South University of Science and Technology of China, Shenzhen, Guangdong 518055, P. R. China*

[4]*Collaborative Innovation Center of Advanced Aero-Engine, Beijing 100191, P. R. China*

(Dated: June 10, 2016)

We investigate energy transfer across scales in three-dimensional compressible magnetohydrodynamic (MHD) turbulence, a model often used to study space and astrophysical plasmas. Analysis shows that the kinetic and magnetic energy cascades conservatively from large to small scales in cases with varying degrees of compression. With more compression, energy fluxes due to the pressure dilation and subscale mass flux are greater, but conversion between kinetic and magnetic energy by magnetic line stretching is less efficient. Energy transfer between the same fields is dominated by local contributions regardless of compressive effects. In contrast, the conversion between kinetic and internal energy by pressure dilation is dominated by the largest-scale contributions. Energy conversion between the velocity and magnetic fields is weakly local.

The statistical properties of turbulence underlie many physical processes in both astrophysical and geophysical systems. In particular, there is growing evidence is that strongly compressible turbulence plays a role in amplification of magnetic fields[1], and possibly the production of energetic particles [2, 3], especially near shocks [4]. Meanwhile decades of evidence suggest that the paradigm of the incompressible cascade is of great significance in understanding turbulence in apparently compressible plasmas such as the solar wind and interstellar medium [5–7]. While the reconciliation of these views is often based on hierarchical arguments or assumptions about cascade [8–10], a more fundamental perspective requires a detailed understanding of the cascade in compressible plasmas. The present paper addresses statistical properties of energy transfer across scales in the familiar but less studied compressible magnetohydrodynamics (MHD) model. The best studied case, the Kolmogorov phenomenology of incompressible hydrodynamic (HD) turbulence [11], assumes the locality of energy transfer across scales. An inertial range emerges in which the statistics are independent of the large and small scales in the system. Energy transfer across scales in HD turbulence has been well studied, and its locality has been verified, see [12–23]. This issue is less well understood in MHD turbulence, which involves both velocity and magnetic fields, several energy transfers between the different fields, and greater opportunities for nonlocal interactions in scale.

The energy transfer in incompressible MHD turbulence has been extensively investigated [24–30], including use of Fourier-space shell models [31–37] to estimate scale to scale energy fluxes. Some results suggest that energy transfer between the same fields is fairly local, but transfer between different fields is highly non-local. Recent work [38] employing a coarse-graining approach showed scale locality of flux of the total energy and for the conversion of kinetic and magnetic energy, and explained the disagreement with the result obtained with the shell-to-shell model [33]. However, no similar studies exist for the compressible MHD turbulence.

In this letter we use high-resolution direct numerical simulation of mechanically forced compressible MHD turbulence to study the energy transfer between different scales and fields. We introduce several energy transfer functions with filtering approaches and analyze their statistical properties and scale locality. A comparison of the energy-transfer from simulations differing only in the forcing mechanism would clearly illustrate the effects of compression. The numerical simulation employs a hybrid compact-WENO scheme [39] in a $(2\pi)^3$ domain, with a resolution of 512^3 grid points, Reynolds number $Re = 500$, magnetic Reynolds number $Re_m = 500$ and Mach number $Ma = 0.3$. The velocity field can be decomposed into a solenoidal part $\boldsymbol{u}_s$ and a compressive part $\boldsymbol{u}_c$, $\boldsymbol{u} = \boldsymbol{u}_s + \boldsymbol{u}_c$, where $\nabla \cdot \boldsymbol{u}_s = 0$ and $\nabla \times \boldsymbol{u}_c = 0$, as well as the kinetic energy, say $E_k = E_s + E_c$. The large-scale force (see, e.g., [40]) consists of holding constant in time the velocity modes (and energies) in the first two wavenumber shells $0.5 \le |\boldsymbol{k}| \le 1.5$ and $1.5 \le |\boldsymbol{k}| \le 2.5$. Writing each of these modes as $\hat{\boldsymbol{u}}^*(\boldsymbol{k}) = l_s \hat{\boldsymbol{u}}_s(\boldsymbol{k}) + l_c \hat{\boldsymbol{u}}_c(\boldsymbol{k})$, we specify the ratio $r_s/r_c = [(l_s^2 - 1)E_s]/[(l_c^2 - 1)E_c]$, which determines l_s and l_c, thus controlling the amount of compression. More details of the driving are referred to [39]. We study here two cases (see Table I): pure solenoidal forcing ($r_c = 0$, i.e. Run 1) and simultaneous solenoidal and compressive forcing ($r_s/r_c = 1/2$, i.e. Run 2) cases. The initial conditions are the same for the two cases. The initial kinetic and magnetic energies are equal, and the initial cross helicity, though not exactly zero, can be considered as negligible. No uniform magnetic field is imposed externally.

The compressive ratio, $R_c = \langle\theta^2\rangle/(\langle\theta^2\rangle+\langle|\boldsymbol{\omega}|^2\rangle)$, where θ is the dilation and $\boldsymbol{\omega}$ is the vorticity, and the normalized density fluctuation, $\delta\rho'/\langle\rho\rangle = \sqrt{\langle(\rho-\langle\rho\rangle)^2\rangle}/\langle\rho\rangle$ are much larger in Run 2, which is forced with a compressive component. Note that $\langle\cdots\rangle$ denotes a space-time average over the entire domain, and for a time in which flow is approximately stationary (about 4 large scale turnover times). Fig. 1(a),(b) show that the magnetic and kinetic energies are comparable at most scales. The shear velocity dominates for solenoidal forcing (see Fig. 1(a)). The solenoidal velocity and the magnetic fields exhibit a $\sim k^{-5/3}$ spectrum, while the compressive velocity shows a $\sim k^{-2}$ spectrum in the more compressive case (Fig. 1(b)) due to the formation of large-scale shock waves, which are evident in Fig. 1(c) where the sharp jump represent the large gradient of density.

TABLE I. Characteristic parameters

Cases	r_s	r_c	Re_λ	M_t	R_c	$\delta\rho'/\langle\rho\rangle$
Run 1	1.0	0.0	210	0.66	0.007	0.17
Run 2	1.0	2.0	150	0.68	0.29	0.43

To investigate cross scale energy transfer, we resolve fields both in space and in scale using a simple filtering approach [19, 41]. The low-pass filtered field, which only contains information at length scales $>\ell$, is defined as $\bar{\boldsymbol{a}}_\ell(\boldsymbol{x}) = \int d^3\boldsymbol{r} G_\ell(\boldsymbol{r})\, \boldsymbol{a}(\boldsymbol{x}+\boldsymbol{r})$, where $G_\ell(\boldsymbol{r}) = \ell^{-3}G(\boldsymbol{r}/\ell)$ is a filtering kernel and $G(\boldsymbol{r})$ is a normalized boxcar window function. In equations with variable density, we apply a Favre filter (density-weighted filter) $\tilde{\boldsymbol{a}}_\ell = \overline{(\rho\boldsymbol{a})}_\ell/\bar\rho_\ell$ [42]. The filtered equations for the large-scale kinetic energy $\tilde{E}_k = \bar\rho_\ell|\tilde{\boldsymbol{u}}_\ell|^2/2$ and large-scale magnetic energy $\bar{E}_m = |\bar{\boldsymbol{b}}_\ell|^2/2$ read

$$\frac{\partial \tilde{E}_k}{\partial t} + \nabla\cdot\boldsymbol{J}^u_\ell = -\boldsymbol{\Pi}^u_\ell - \boldsymbol{\Lambda}_\ell - \boldsymbol{\Phi}_\ell - \boldsymbol{T}_{1,\ell} - \boldsymbol{T}_{2,\ell} - \boldsymbol{D}^u_\ell, \quad (1a)$$

$$\frac{\partial \bar{E}_m}{\partial t} + \nabla\cdot\boldsymbol{J}^b_\ell = -\boldsymbol{\Pi}^b_\ell + \boldsymbol{T}_{1,\ell} + \boldsymbol{T}_{2,\ell} - \boldsymbol{D}^b_\ell, \quad (1b)$$

where $\boldsymbol{J}^u_\ell$ and $\boldsymbol{J}^b_\ell$ represent the spatial transport of energies; $\boldsymbol{\Pi}^u_\ell = -\left(\bar\rho_\ell\tilde{\boldsymbol{\tau}}^u_\ell + \bar{\boldsymbol{\tau}}^b_\ell\right) : \nabla\tilde{\boldsymbol{u}}_\ell$, where ":" is a double dot product, $\tilde{\boldsymbol{\tau}}^u_\ell = \left[\widetilde{(\boldsymbol{uu})}_\ell - \tilde{\boldsymbol{u}}_\ell\tilde{\boldsymbol{u}}_\ell\right]$ is the subscale Reynolds stress, $\bar{\boldsymbol{\tau}}^b_\ell = -\left[\overline{(\boldsymbol{bb})}_\ell - \bar{\boldsymbol{b}}_\ell\bar{\boldsymbol{b}}_\ell\right] + \frac{1}{2}\left[\overline{(\boldsymbol{b}^2)}_\ell - \bar{\boldsymbol{b}}^2_\ell\right]\mathbf{I}$ is the subscale magnetic stress, and $\mathbf{I}$ is the unity tensor. $\boldsymbol{\Lambda}_\ell = \bar\rho_\ell^{-1}\bar{\boldsymbol{\tau}}^\rho_\ell \cdot \left[\nabla\cdot\left(\bar p_\ell\mathbf{I} + \frac{1}{2}\bar{\boldsymbol{b}}^2_\ell\mathbf{I} - \bar{\boldsymbol{b}}_\ell\bar{\boldsymbol{b}}_\ell\right)\right]$, where $\bar{\boldsymbol{\tau}}^\rho_\ell = \left[\overline{(\rho\boldsymbol{u})}_\ell - \bar\rho_\ell\bar{\boldsymbol{u}}_\ell\right]$ is the subscale mass flux. The large-scale forcing term is eliminated here. $\boldsymbol{\Pi}^b_\ell = -\bar{\boldsymbol{\epsilon}}_\ell\cdot(\nabla\times\bar{\boldsymbol{b}}_\ell)$ is the magnetic energy flux across scale l, and $\bar{\boldsymbol{\epsilon}}_\ell = \left[\overline{(\boldsymbol{u}\times\boldsymbol{b})}_\ell - \bar{\boldsymbol{u}}_\ell\times\bar{\boldsymbol{b}}_\ell\right]$ is the subscale electromotive force;

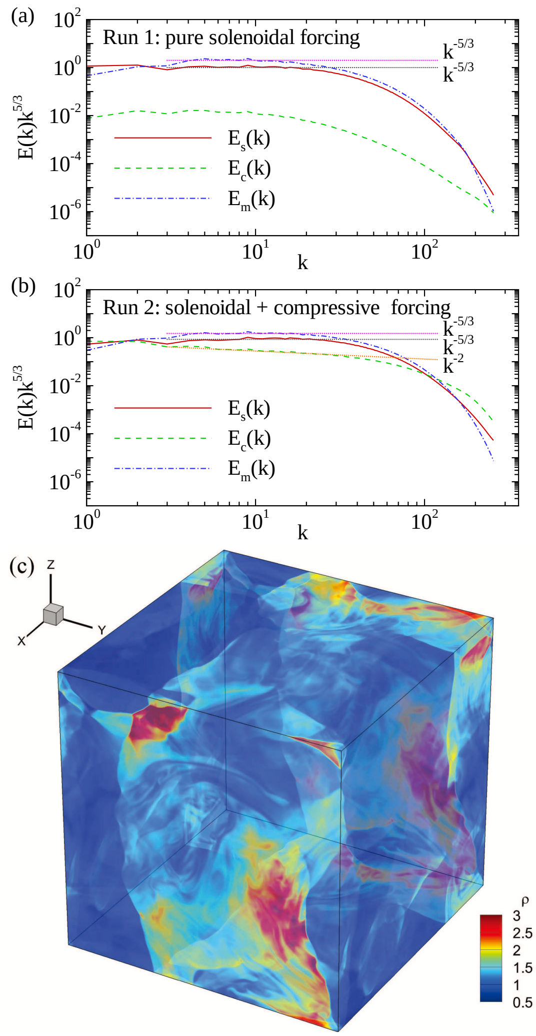

FIG. 1. Spectra compensated with $k^{5/3}$ from Run 1 (a) and Run 2 (b) for solenoidal kinetic energy $E_s(k)$, compressive kinetic energy $E_c(k)$ and magnetic energy $E_m(k)$. The dotted lines indicate the $k^{-5/3}$ and k^{-2} spectra. Run 2 is more compressive. (c) Contour of density from Run 2.

$\boldsymbol{\Phi}_\ell = -\bar p_\ell\nabla\cdot\bar{\boldsymbol{u}}_\ell$ is the pressure dilation; $\boldsymbol{T}_{1,\ell} = -\frac{1}{2}\bar{\boldsymbol{b}}^2_\ell\nabla\cdot\bar{\boldsymbol{u}}_\ell$ and $\boldsymbol{T}_{2,\ell} = \bar{\boldsymbol{b}}_\ell\cdot\nabla\bar{\boldsymbol{u}}_\ell\cdot\bar{\boldsymbol{b}}_\ell$ represent an exchange of large-scale kinetic and magnetic energy by compression and large-scale magnetic line stretching, respectively; $\boldsymbol{D}^u_\ell$ and $\boldsymbol{D}^b_\ell$ are the viscous and Ohmic dissipation terms, respectively. Note that $\boldsymbol{\Phi}_\ell$, $\boldsymbol{T}_{1,\ell}$ and $\boldsymbol{T}_{2,\ell}$ incorporate information only from scales $>\ell$. Therefore, they are insensitive to excitations at scales $<\ell$ and do not contribute to the transfer of energy across scale ℓ. In contrast, $\boldsymbol{\Pi}^u_\ell$, $\boldsymbol{\Lambda}_\ell$ and $\boldsymbol{\Pi}^b_\ell$ depend on fluctuations at scales $<\ell$ and are therefore capable of direct transfer of energy across scales.

We show different energy fluxes in Fig. 2. The fluxes are normalized by the total viscous and Ohmic dissipation, $\epsilon_T = \langle\epsilon_u\rangle + \langle\epsilon_b\rangle = \langle\sigma_{ij}\partial_j u_i\rangle + \langle\eta\partial_i b_j\partial_i b_j\rangle$, where $\sigma_{ij} = \mu(\partial_i u_j + \partial_j u_i) - \frac{2}{3}\mu\theta\delta_{ij}$, μ is the dynamic viscosity, and η is the electrical conductivity. The filtering scale is normalized by the Kolmogorov length scale $\eta_k = \left[\langle \mu/\rho\rangle^3/\langle \epsilon_u/\rho\rangle\right]^{1/4}$. The total energy (kinetic and magnetic energy) can be converted into internal energy by the pressure-dilation work $-\langle p\nabla\cdot\boldsymbol{u}\rangle$ and the total dissipation ϵ_T. A part of the large-scale total energy $\langle \tilde{E}_k + \bar{E}_m\rangle$ is transferred across scale ℓ to the small-scale total energy by the positive flux $\langle \boldsymbol{\Pi}_\ell^u + \boldsymbol{\Pi}_\ell^b + \boldsymbol{\Lambda}_\ell\rangle$, which will finally be dissipated at the dissipation scale by ϵ_T. Therefore, $\langle \boldsymbol{\Pi}_\ell^u + \boldsymbol{\Pi}_\ell^b + \boldsymbol{\Lambda}_\ell\rangle \sim \epsilon_T$, as shown in Fig. 2(a)(b). Since the dissipation terms $\langle \boldsymbol{D}_\ell^u\rangle$ and $\langle \boldsymbol{D}_\ell^b\rangle$ are small but can not be fully neglected, $\langle \boldsymbol{\Pi}_\ell^u + \boldsymbol{\Pi}_\ell^b + \boldsymbol{\Lambda}_\ell\rangle/\epsilon_T$ is slightly less than 1. There is an inertial range over which the fluxes $\langle \boldsymbol{\Pi}_\ell^u + \boldsymbol{\Pi}_\ell^b\rangle$, $\langle \boldsymbol{\Lambda}_\ell\rangle$ and $\langle \boldsymbol{\Phi}_\ell\rangle$ are almost constant in both cases. The terms $\langle \boldsymbol{\Pi}_\ell^{u,b}\rangle$ transfer energy from large to small scale due to interaction of subscale stresses with large-scale fields. In contrast, $\langle \boldsymbol{\Lambda}_\ell\rangle$ represents interaction of subscale mass flux with large-scale pressure gradient and (when negative) transfers energy from small to large scale.

Note that $\langle \boldsymbol{\Lambda}_\ell\rangle$ in Fig. 2(a) is vanishingly small due to the fact that the subscale mass flux $\bar{\boldsymbol{\tau}}_\ell^\rho = \left[\overline{(\rho\boldsymbol{u})}_\ell - \bar{\rho}_\ell \bar{\boldsymbol{u}}_\ell\right]$ is negligible in Run 1, with pure solenoidal forcing. The pressure dilation $\langle \boldsymbol{\Phi}_\ell\rangle$ is also very small in this case. Overall, we see that Run 1 behaves like a nearly incompressible flow. In contrast, in Run 2 (Fig. 2(b)), the rate of kinetic energy conversion into internal energy by the pressure dilation $\langle \boldsymbol{\Phi}_\ell\rangle$ is merely 30% smaller than the total dissipation ϵ_T. Therefore, in the moderately compressive flow, apart from the viscous dissipation, which is the only way to convert kinetic to internal energy in the incompressible flow, the pressure dilation can also effectively couple kinetic with internal energy.

The exchange between kinetic and magnetic energy is not a conservative cascade, and $\langle \boldsymbol{T}_{1,\ell}\rangle$ and $\langle \boldsymbol{T}_{2,\ell}\rangle$ decrease with increasing filtering scale ℓ (see Fig. 2(c)). The magnitude of $\langle \boldsymbol{T}_{1,\ell}\rangle$ related to compressions is smaller than that of $\langle \boldsymbol{T}_{2,\ell}\rangle$ related to vortex structures in both cases. The dynamo process excited by vortices is therefore more efficient than that excited by compressions, a conclusion consistent with the result [43] that coherent vortical motions are necessary to drive an efficient dynamo. In comparing Run 1 and Run 2, one observes that $\langle \boldsymbol{T}_{2,\ell}\rangle$ is larger in Run 1, because pure solenoidal forcing excites more vorticity (see Table I) and thus tangles the magnetic field more strongly. In contrast, $\langle \boldsymbol{T}_{1,\ell}\rangle$ in Run 2 is larger due to more compression.

In order to clarify the effects of compressibility on the locality of energy flux, we only investigate the more compressive case (see Run 2) hereinafter and compare with the existing results in the incompressible MHD turbulence (see [31–38]). For the energy flux across any scale ℓ, if the contribution from scale $\Delta \gg \ell$ is negligible, the energy flux is infrared local; if the contribution from scale $\delta \ll \ell$ is negligible, the energy flux is ultraviolet local [19]. We use the magnetic energy flux $\boldsymbol{\Pi}_\ell^b = -\bar{\boldsymbol{\epsilon}}_\ell \cdot \left(\nabla\times\bar{\boldsymbol{b}}_\ell\right)$ to illustrate the definition. Let $\bar{\boldsymbol{a}}_{\Delta^{(n)}}$ be the low-pass filtered field with the filtering scale $\Delta^{(n)} = (1.25)^n \ell, (n = 0,1,2,\cdots)$. The corresponding high-pass filtered field is $\boldsymbol{a}'_{\Delta^{(n)}} = \boldsymbol{a} - \bar{\boldsymbol{a}}_{\Delta^{(n)}}$. We then obtain the contribution to the flux across scale ℓ from scales $> \Delta^{(n)}$ as

$$\boldsymbol{\Pi}_\ell^{b,>\Delta^{(n)}} = -\bar{\boldsymbol{\epsilon}}_\ell\left(\bar{\boldsymbol{u}}_{\Delta^{(n)}}, \bar{\boldsymbol{b}}_{\Delta^{(n)}}\right)\cdot\left[\nabla\times\overline{\left(\bar{\boldsymbol{b}}_{\Delta^{(n)}}\right)}_\ell\right], \quad (2)$$

where $\bar{\boldsymbol{\epsilon}}_\ell\left(\bar{\boldsymbol{u}}_{\Delta^{(n)}}, \bar{\boldsymbol{b}}_{\Delta^{(n)}}\right) = \overline{\left(\bar{\boldsymbol{u}}_{\Delta^{(n)}}\times\bar{\boldsymbol{b}}_{\Delta^{(n)}}\right)}_\ell - \overline{\left(\bar{\boldsymbol{u}}_{\Delta^{(n)}}\right)}_\ell \times \overline{\left(\bar{\boldsymbol{b}}_{\Delta^{(n)}}\right)}_\ell$. The contribution from scales $> \Delta^{(0)} = \ell$ can be further split into shells $\boldsymbol{\Pi}_\ell^{b,\Delta^{(n)}}, (n = 0,1,2,\cdots)$,

$$\boldsymbol{\Pi}_\ell^{b,\Delta^{(n)}} = \boldsymbol{\Pi}_\ell^{b,>\Delta^{(n)}} - \boldsymbol{\Pi}_\ell^{b,>\Delta^{(n+1)}}. \quad (3)$$

Each shell $\boldsymbol{\Pi}_\ell^{b,\Delta^{(n)}}$ is quantified by the contribution from scales $\left[\Delta^{(n)}, \Delta^{(n+1)}\right]$. Similarly, the contribution to the flux across scale ℓ from scales $< \delta^{(n)} = (1.25)^{-n}\ell$ can be

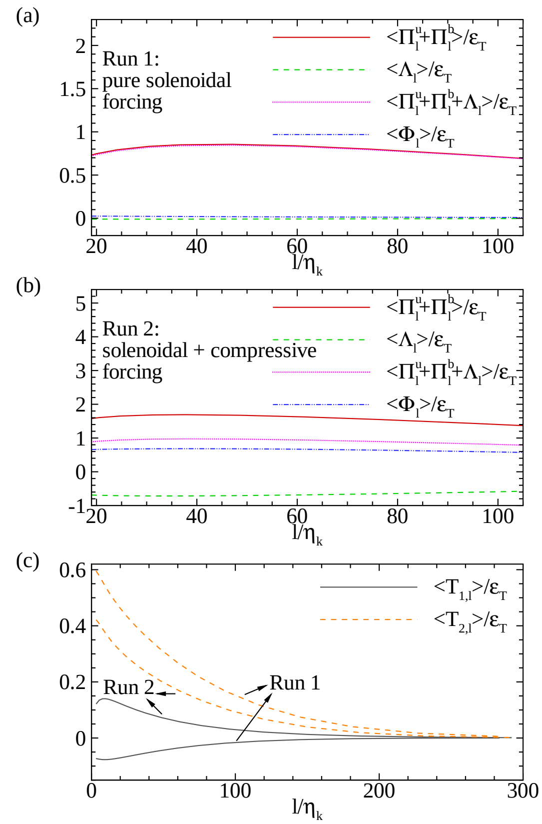

FIG. 2. Different energy fluxes from Run 1 (a) and Run 2 (b) as a function of filtering length ℓ. The total energy flux remains fairly constant over the inertial range. The pressure dilation $\langle \boldsymbol{\Phi}_\ell\rangle$ and subscale mass flux term $\langle \boldsymbol{\Lambda}_\ell\rangle$ are negligible in Run 1 due to less compression. (c) the energy exchange between kinetic and magnetic energy. The dynamo related to vortices (i.e. $\langle \boldsymbol{T}_{2,\ell}\rangle$) is more efficient than that related to compressions (i.e. $\langle \boldsymbol{T}_{1,\ell}\rangle$).

written as:

$$\mathbf{\Pi}_\ell^{b,<\delta^{(n)}} = -\bar{\boldsymbol{\epsilon}}_\ell\left(\boldsymbol{u'}_{\delta^{(n)}}, \boldsymbol{b'}_{\delta^{(n)}}\right) \cdot \left(\nabla \times \bar{\boldsymbol{b}}_\ell\right). \tag{4}$$

Note that if we were to replace the last term, $\bar{\boldsymbol{b}}_\ell$, with the quantity $\overline{(\boldsymbol{b'}_{\delta^{(n)}})}_\ell$, then Eq. (4) would be guaranteed to be vanishingly small because $\overline{(\boldsymbol{b'}_{\delta^{(n)}})}_\ell \sim 0$. So using $\bar{\boldsymbol{b}}_\ell$ directly in this term can help to figure out the ultraviolet locality of the energy flux due to subscale stress more clearly. Then

$$\mathbf{\Pi}_\ell^{b,\delta^{(n)}} = \mathbf{\Pi}_\ell^{b,<\delta^{(n)}} - \mathbf{\Pi}_\ell^{b,<\delta^{(n+1)}}, \tag{5}$$

is the contribution from scales $\left[\delta^{(n+1)}, \delta^{(n)}\right]$. The contribution to $\mathbf{\Pi}_\ell^u$, $\mathbf{\Lambda}_\ell$, $\mathbf{\Phi}_\ell$, $\boldsymbol{T}_{1,\ell}$ and $\boldsymbol{T}_{2,\ell}$ from different scale shells can be obtained in a similar way.

Fig. 3(a) shows the normalized contribution to the magnetic energy flux across scale ℓ from different scale shells, $\langle\mathbf{\Pi}_\ell^{b,\Delta^{(n)}}\rangle/\langle\mathbf{\Pi}_\ell^b\rangle$ and $\langle\mathbf{\Pi}_\ell^{b,\delta^{(n)}}\rangle/\langle\mathbf{\Pi}_\ell^b\rangle$. For any fixed scale ℓ, the contribution is found to be locally maximum along the diagonal line, which means that the magnetic energy flux across length scale ℓ is dominated by the contributions from scales close to ℓ. Thus the cascade of magnetic energy due to the subscale stresses is local. In order to get a better understanding of the transfer, we choose a length-scale ℓ in the inertial range, eg. $\ell/\eta_k \sim 50$, and shown in Fig. 3(b). It's obvious that the contributions maximize at $n \sim 0$, i.e. scales $\Delta \sim \ell$ and $\delta \sim \ell$, and decrease rapidly at far-away scales. Both the infrared locality and ultraviolet locality hold for $\mathbf{\Pi}_\ell^b$. The cascades of kinetic energy through $\mathbf{\Pi}_\ell^u$ and $\mathbf{\Lambda}_\ell$, which are not shown here, are local as well.

Because $\mathbf{\Phi}_\ell$, $\boldsymbol{T}_{1,\ell}$ and $\boldsymbol{T}_{2,\ell}$ incorporate information only from scales $> \ell$, infrared locality is quantified from these fluxes; see Fig. 3(c). The pressure dilation $\langle\mathbf{\Phi}_\ell\rangle$ represents the conversion of kinetic energy to internal energy through compression. Fig. 3(c) shows the contributions due to $\langle\mathbf{\Phi}_\ell\rangle$ filtered at various scales, and one sees that the largest scales (largest n), make the most significant contributions, as in compressible HD turbulence [44, 45]. With the influence of pressure dilation mainly at the largest scales, the inertial range scaling law is relatively free of compressive effects, and kinetic and internal energy can decouple in the inertial range. Finally we recall that incompressible MHD studies [33] suggested that the exchange between kinetic and magnetic energy is highly non-local. In contrast, our results show weak infrared locality of the magnetic line stretching term, $\boldsymbol{T}_{2,\ell}$ and the dilation term, $\boldsymbol{T}_{1,\ell}$. Most of the fluxes result from bands $n = 0 \sim 5$, i.e. scales $\ell \sim 3\ell$. This disparity may emerge from methodological differences, as suggested previously [38].

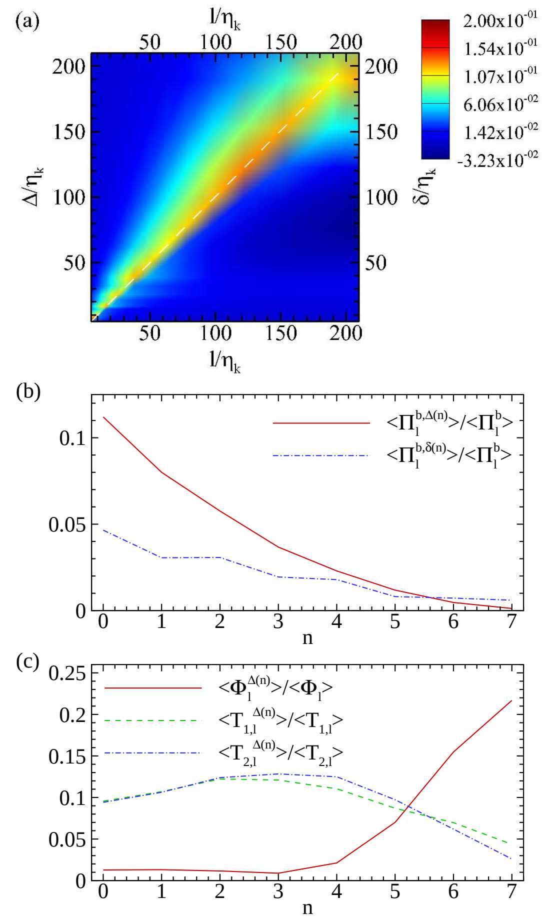

FIG. 3. (a) The normalized contribution to the magnetic energy flux across scale ℓ, $\langle\mathbf{\Pi}_\ell^b\rangle$ from different scale shells. The upper left part has vertical axis labeled Δ/η_k and the lower right part has a vertical axis labeled δ/η_k. (b) The normalized contribution to magnetic energy flux across scale $\ell/\eta_k \sim 50$ from different size bands, where $\Delta^{(n)} = (1.25)^n\,\ell$ and $\delta^{(n)} = (1.25)^{-n}\,\ell$. (c) The normalized contribution from different scale shells to the conversion of kinetic to internal energy, $\mathbf{\Phi}_\ell$, and the conversion of kinetic to magnetic energy, $\boldsymbol{T}_{1,\ell}$, $\boldsymbol{T}_{2,\ell}$. Only contributions from $\Delta^{(n)}$ are calculated. ℓ/η_k and $\Delta^{(n)}$ are the same as (b). The quantities plotted here are specifically for Run 2.

In this paper, we analyze the energy transfer of compressible MHD turbulence in real space. We find an apparent inertial range over which conservative energy cascade of the velocity and magnetic fields occurs, regardless of the forcing mechanism, almost completely decoupled from pressure dilation effects. For a higher degree of compression, more kinetic energy is converted into the internal energy by the pressure dilation, presumably through shock-like structures (see Fig. 1c). However, less vorticity generated in the more compressive case leads to less efficient magnetic dynamo by magnetic line stretching. Kinetic and magnetic energy cascades are local, while the conversion between kinetic and magnetic energy is weakly local. Conversion between kinetic and internal energy by the pressure dilation occurs mainly at the largest scales.

Although our results are based on the numerical simulation with no background magnetic field and of moderate Re number much smaller than that in many astrophysical plasmas and laboratory situations, it represents an important step towards understanding physical processes such as heating and possible production of energetic particles. In the case of a low collisionality plasma, for which MHD is often used as a leading order approximation, heating and the production of entropy will occurs mainly at small scales. The fluxes of energy through the channels of velocity field, magnetic field and pressure dilation, which we have examined in some detail here, will act as small scale drivers for kinetic processes that absorb these fluxes and energize particles. Many additional questions arise, including for example an assessment of the effects of background magnetic field, larger Re number and varying Mach number, and these will warrant further study.

We acknowledge useful discussions with Kun Yang. This work has been supported by the National Science Foundation of China (NSFC Grant Nos. 11221062, 91130001 and U1330107), and by NASA grant NNX14AI63G (Heliophysics Grand Challenge) and US National Science Foundation grants AGS-1063439 (Solar Terrestrial) and AGS-1156094 (SHINE). The support provided by the China Scholarship Council during a visit of Yan Yang to University of Delaware is acknowledged. The simulations were done on the TH-1A super-computer in Tianjin, China. This research was also supported in part through the use of Information Technologies (IT) resources at the University of Delaware, specifically the high-performance computing resources.

* syp@mech.pku.edu.cn
† wanmp@sustc.edu.cn

[1] J. Giacalone and J. R. Jokipii, Astrophys. J. **663**, L41 (2007).
[2] J. R. Jokipii and M. A. Lee, Astrophys. J. **713**, 475 (2010).
[3] L. A. Fisk and G. Gloeckler, Space Sci. Rev. **173**, 433 (2012).
[4] Y. Matsumoto, T. Amano, T. N. Kato, and M. Hoshino, Science **347**, 974 (2015).
[5] P. J. Coleman Jr., Astrophys. J. **153**, 371 (1968).
[6] J. W. Armstrong, J. M. Cordes, and B. J. Rickett, Nature **291**, 561 (1981).
[7] O. Alexandrava, C. H. K. Chen, L. Sorriso-Valvo, T. S. Horbury, and S. D. Bale, Space Sci. Rev. **178**, 101 (2013).
[8] D. Montgomery, M. R. Brown, and W. H. Matthaeus, J. Geophys. Res. **92(A1)**, 282 (1987).
[9] G. P. Zank and W. H. Matthaeus, J. Geophys. Res. **97(A11)**, 17189 (1992).
[10] P. Goldreich and S. Sridhar, Astrophys. J. **438**, 763 (1995).
[11] A. N. Kolmogorov, Dokl. Akad. Nauk SSSR **30**, 299 (1941).
[12] J. A. Domaradzki, Phys. Fluids **31**, 2747 (1988).
[13] J. A. Domaradzki and R. S. Rogallo, Phys. Fluids A **2**, 413 (1990).
[14] K. Ohkitani and S. Kida, Phys. Fluids A **4**, 794 (1992).
[15] Y. Zhou, Phys. Fluids A **5**, 1092 (1993).
[16] Y. Zhou, Phys. Fluids A **5**, 2511 (1993).
[17] G. L. Eyink, Physica D **78**, 222 (1994).
[18] K. Kishida, K. Araki, S. Kishiba, and K. Suzuki, Phys. Rev. Lett. **83**, 5487 (1999).
[19] G. L. Eyink, Physica D **207**, 91 (2005).
[20] J. A. Domaradzki and D. Carati, Phys. Fluids **19**, 085112 (2007).
[21] J. A. Domaradzki and D. Carati, Phys. Fluids **19**, 085111 (2007).
[22] G. L. Eyink and H. Aluie, Phys. Fluids **21**, 115107 (2009).
[23] H. Aluie and G. L. Eyink, Phys. Fluids **21**, 115108 (2009).
[24] G. Dar, M. K. Verma, and V. Eswaran, Physica D **157**, 207 (2001).
[25] O. Schilling and Y. Zhou, J. Plasma Phys. **68**, 389 (2002).
[26] A. A. Schekochihin, S. C. Cowley, S. F. Taylor, J. L. Maron, and J. C. McWilliams, Astrophys. J. **612**, 276 (2004).
[27] M. K. Verma, Phys. Rep. **401**, 229 (2004).
[28] A. Alexakis, B. Bigot, H. Politano, and S. Galtier, Phys. Rev. E **76**, 056313 (2007).
[29] T. A. Yousef, F. Rincon, and A. A. Schekochihin, J. Fluid Mech. **575**, 111 (2007).
[30] J. Cho, Astrophys. J. **725**, 1786 (2010).
[31] M. K. Verma, A. Ayyer, and A. V. Chandra, Phys. Plasmas **12**, 082307 (2005).
[32] O. Debliquy, M. K. Verma, and D. Carati, Phys. Plasmas **12**, 042309 (2005).
[33] A. Alexakis, P. D. Mininni, and A. Pouquet, Phys. Rev. E **72**, 046301 (2005).
[34] D. Carati, O. Debliquy, B. Knaepen, B. Teaca, and M. Verma, J. Turbul. **7**, 51 (2006).
[35] A. Alexakis, P. D. Mininni, and A. Pouquet, New J. Phys. **9**, 298 (2007).
[36] J. A. Domaradzki, B. Teaca, and D. Carati, Phys. Fluids **22**, 051702 (2010).
[37] B. Teaca, D. Carati, and J. A. Domaradzki, Phys. Plasmas **18**, 112307 (2011).
[38] H. Aluie and G. L. Eyink, Phys. Rev. Lett. **104**, 081101 (2010).
[39] Y. Yang, M. Wan, Y. Shi, K. Yang, and S. Chen, J. Comput. Phys. **306**, 73 (2016).
[40] S. Chen, G. D. Doolen, R. H. Kraichnan, and Z.-S. She, Phys. Fluids A **5**, 458 (1993).
[41] M. Germano, J. Fluid Mech. **238**, 325 (1992).
[42] A. Favre, J. Mec. **4**, 361 (1965).
[43] C.Federrath, G. Chabrier, J. Schober, R. Banerjee, R. S. Klessen, and D. R. G. Schleicher, Phys. Rev. Lett. **107**, 114504 (2011).
[44] H. Aluie, Phys. Rev. Lett. **106**, 174502 (2011).
[45] H. Aluie, S. Li, and H. Li, Astrophys. J. Lett. **106**, 174502 (2012).